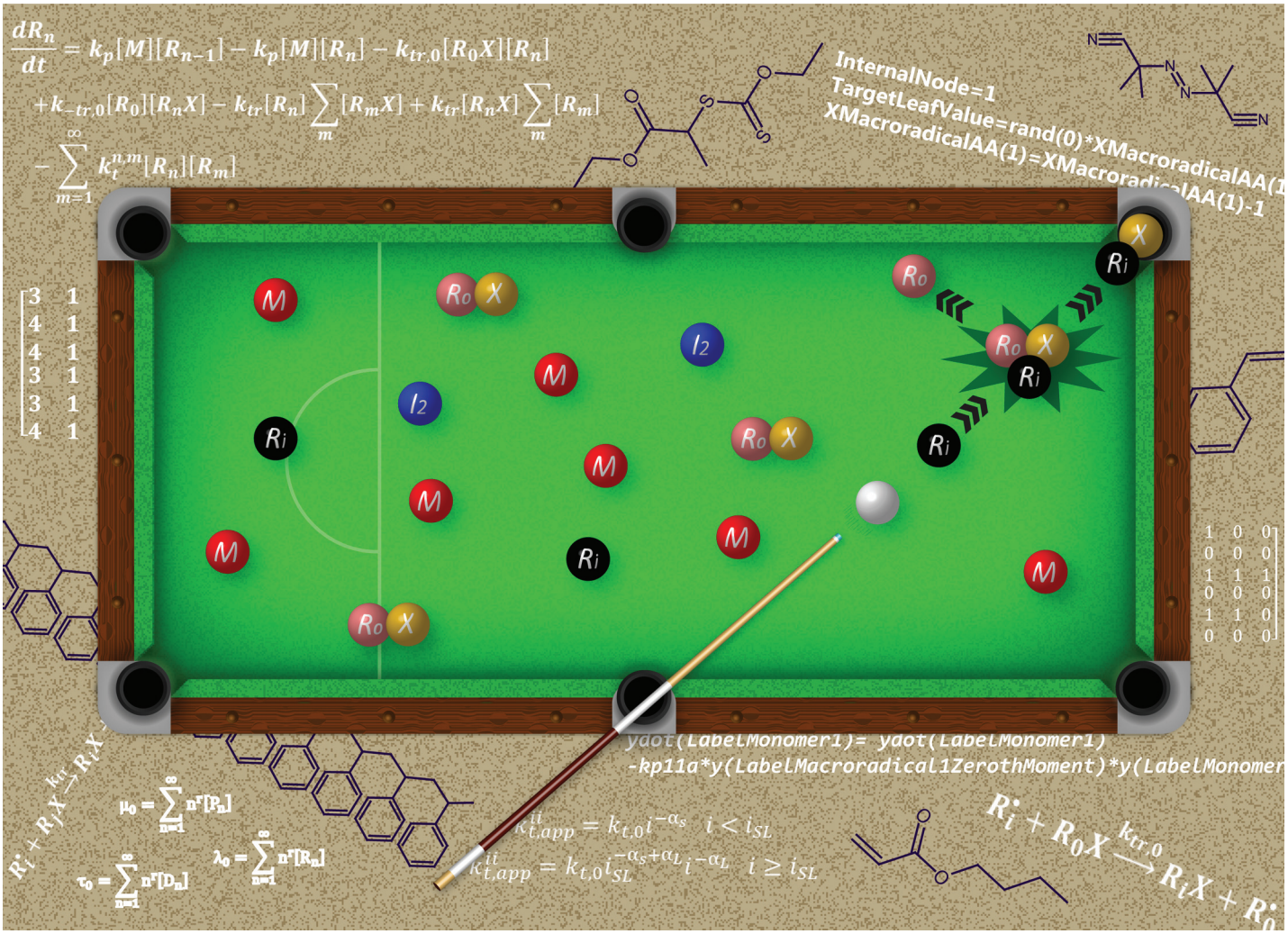

Highlighting research from Laboratory for Chemical Technology (LCT), Ghent University.

A detailed mechanistic study of bulk MADIX of styrene and its chain extension

The microstructural evolution of individual macrospecies during MADIX of styrene and its chain extension with fresh styrene or *n*-butyl acrylate is visualised *in silico*. This allows an unbiased (co)polymer product quality labelling according to monomer sequences and end-groups. Novel mechanistic insights are obtained based on model analysis.

As featured in:

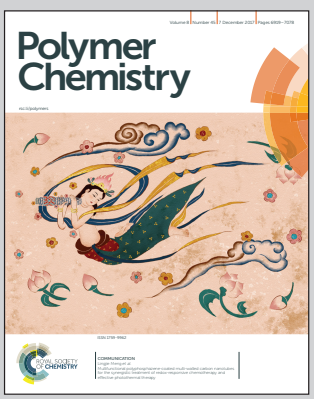

See Dagmar R. D'hooge *et al.*, *Polym. Chem.*, 2017, **8**, 6948.

ROYAL SOCIETY OF CHEMISTRY

rsc.li/polymers

Registered charity number: 207890

Polymer Chemistry

PAPER

Cite this: *Polym. Chem.*, 2017, **8**, 6948

A detailed mechanistic study of bulk MADIX of styrene and its chain extension†

Dries J. G. Devlaminck,[a] Paul H. M. Van Steenberge,[a] Lies De Keer,[a] Marie-Françoise Reyniers[a] and Dagmar R. D'hooge*[a,b]

Received 10th June 2017,
Accepted 14th October 2017

DOI: 10.1039/c7py00961e

rsc.li/polymers

The microstructural evolution of individual macrospecies during bulk macromolecular design by interchange of xanthates (MADIX) of styrene with (*O*-ethyl xanthate)-2-ethyl propionate as an initial agent (R_0X) and its chain extension with fresh styrene or *n*-butyl acrylate (*n*BuA) is visualized *in silico*, allowing an unbiased (co)polymer product quality labelling according to monomer sequences and end-groups. Degenerative transfer coefficients for both exchange with R_0X ($C_{tr,0}$) and macro-RAFT agent (C_{tr}) are reported ($C_{tr,0}$ = 0.80 ± 0.02; C_{tr}: 0.44 ± 0.07) by applying multi-response regression analysis to the experimental data on the RAFT agent and styrene conversion, number and mass average molar masses, and end-group functionality (EGF). The EGF data are obtained by combining dialysis to remove residual R_0X species and elemental analysis. It is shown that the MADIX mechanism can be properly understood only by explicitly acknowledging the differences in exchange reactivities and that the macroradical homopolymer CLD follows a Flory–Schulz distribution, which is an exception for controlled reversible addition–fragmentation chain transfer polymerization. Moreover, for the selected monomer conversion ranges, both "blocks" of the chain extension are formed through a single exchange.

Introduction

One of the major reversible deactivation radical polymerization (RDRP) techniques is reversible addition–fragmentation chain transfer (RAFT) polymerization.[1] Its most relevant elementary reactions are shown in Fig. 1a, assuming for simplicity recombination as the only termination mode and ignoring RAFT cross-termination. As in traditional free radical polymerization (FRP) a conventional radical initiator (I_2) forms initiator fragments (I; blue spheres), which subsequently add to the monomer (M; red spheres), leading to the formation of macroradicals (R_i; i is chain length). In contrast to FRP, these R_i species do not dominantly terminate ((5) in Fig. 1a) to create dead polymer species P but they can also be reversibly deactivated *via* RAFT exchange ((2) and (4) in Fig. 1a).

This RAFT exchange involves a (macro-)RAFT agent (R_iX; $i \geq 0$), resulting in the incorporation of end-group functionality (EGF; yellow cubes in Fig. 1a; X), allowing further chemical modifications such as the preparation of tailored block copolymers.[2–5] In the absence of RAFT degradation reactions[5,6] the amount of X moieties remains constant and under well-defined reaction conditions the number average chain length (x_n) can be tuned by varying the initial molar ratio of the monomer to the RAFT agent ($[M]_0/[R_0X]_0$). The latter ratio is also known as the targeted chain length (TCL), taking into account the fact that the employed I_2 amount is typically negligible.[5]

For most RAFT agents, at low monomer conversions (X_m < 20%), the exchange occurs mainly with the initial RAFT CTA (R_0X; (2) in Fig. 1a), whereas at higher monomer conversions (X_m > 20%) R_0X is no longer present and only macro-RAFT species (R_iX; (4) in Fig. 1a) are involved.[5,7,8] Mechanistically, RAFT exchange is an activation/deactivation process composed of two consecutive elementary reactions, *i.e.* (i) the addition of the (macro-)radical to the S=C group of the (macro-)RAFT agent ($k_{add(,0,a/b)}$ in Fig. 1a) to form an intermediate RAFT radical (INT) and (ii) the fragmentation or βCS-scission ($k_{frag(,0,a/b)}$ in Fig. 1a) of this INT species. In addition, side reactions can occur with particular focus on RAFT cross-termination involving INT species (reactions not shown in Fig. 1a).[9–13]

For an efficient RAFT exchange in which these cross-termination reactions can be ignored, and chain initiation and RAFT fragmentation are sufficiently fast (no inhibition and rate retardation), a so-called degenerative mechanism is formally obtained (Fig. 1b).[14] The introduced (RAFT) transfer "rate coefficients" $k_{tr,0}$, $k_{-tr,0}$, and k_{tr} can be calculated from the elementary RAFT addition and fragmentation rate coefficients

[a]*Laboratory for Chemical Technology (LCT), Ghent University, Technologiepark 914, B-9052 Ghent, Belgium. E-mail: dagmar.dhooge@ugent.be*
[b]*Centre for Textile Science and Engineering, Ghent University, Technologiepark 907, B-9052 Ghent, Belgium*

†Electronic supplementary information (ESI) available. See DOI: 10.1039/c7py00961e

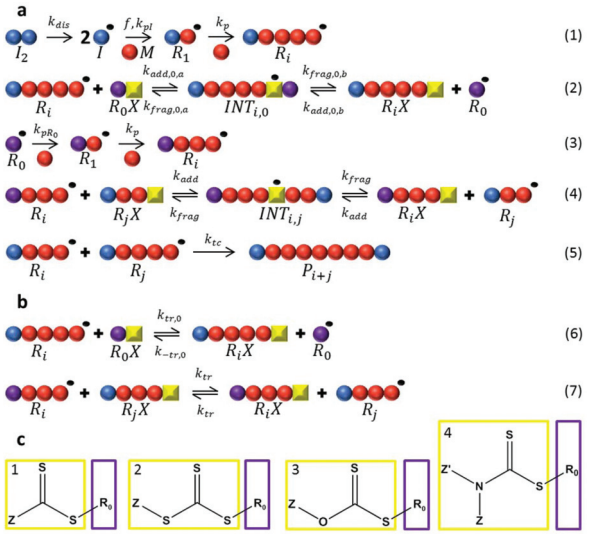

Fig. 1 (a) Key elementary reactions in RAFT polymerization, not displaying for simplicity termination with the RAFT intermediate and conventional termination by disproportionation; I_2: conventional radical initiator, R_0X: initial RAFT agent; I: fragment from I_2; M: monomer; R_0: RAFT leaving group; R_i: macroradical (chain length i); R_iX: dormant macrospecies; $INT_{i,j}$: intermediate RAFT radical (chain length i ("left" arm) and j ("right" arm)); P: dead polymer species; $k_{dis,pl,p,add(0,a/b),frag(0,a/b),pR0,tc}$: rate coefficient for dissociation, chain initiation with I, propagation, RAFT addition, RAFT fragmentation, chain initiation with R_0 and termination by recombination; f: conventional initiator efficiency; (b) formal description of RAFT exchange upon validity of the degenerative RAFT mechanism (eqn (1)–(3)); (c) the main classes of RAFT agents: 1: dithioesters; 2: trithiocarbonates; 3: xanthates; 4: dithiocarbamates.

after the application of the pseudo-steady-state assumption for the calculation of the INT concentrations:[1,5,15,16]

$$k_{\mathrm{tr},0} = k_{\mathrm{add},0,\mathrm{a}} \frac{k_{\mathrm{frag},0,\mathrm{b}}}{k_{\mathrm{frag},0,\mathrm{a}} + k_{\mathrm{frag},0,\mathrm{b}}} = k_{\mathrm{add},0,\mathrm{a}} \varphi_{0,\mathrm{b}} \quad (1)$$

$$k_{-\mathrm{tr},0} = k_{\mathrm{add},0,\mathrm{b}} \frac{k_{\mathrm{frag},0,\mathrm{a}}}{k_{\mathrm{frag},0,\mathrm{a}} + k_{\mathrm{frag},0,\mathrm{b}}} = k_{\mathrm{add},0,\mathrm{b}} \varphi_{0,\mathrm{a}} \quad (2)$$

$$k_{\mathrm{tr}} = \frac{k_{\mathrm{add}}}{2} \quad (3)$$

in which, for simplicity, chain length dependencies have been neglected and $\varphi_{0,\mathrm{a/b}}$ is the fragmentation probability. The ratios of the transfer rate coefficients to their corresponding propagation or chain initiation rate coefficients are known as degenerative RAFT transfer coefficients:[1,5,15,16]

$$C_{\mathrm{tr},0} = \frac{k_{\mathrm{tr},0}}{k_{\mathrm{p}}} \quad (4)$$

$$C_{-\mathrm{tr},0} = \frac{k_{-\mathrm{tr},0}}{k_{\mathrm{pR_0}}} \quad (5)$$

$$C_{\mathrm{tr}} = \frac{k_{\mathrm{tr}}}{k_{\mathrm{p}}} \quad (6)$$

with typical values ranging between 10^{-2} and 10^{4}.[17–19] As a rule of thumb, $C_{\mathrm{tr}(,0)}$ values larger than 10 are necessary to achieve excellent microstructural control (*e.g.* dispersity ($Đ$) < 1.5).[20]

These transfer coefficients are strongly dependent on the chemical structure surrounding the reactive thiocarbonylthio moiety.[15] An overview of the main classes of RAFT agents is provided in Fig. 1c, with the purple/yellow colour boxes for a direct link to Fig. 1a/b. Specifically for xanthates (RAFT agent 3 in Fig. 1c), which contain an oxygen atom at α-position to the thiocarbonylthio functional group, the RAFT transfer capability is strongly reduced. The presence of a delocalizable oxygen electron pair decreases the S=C double-bond character and, consequently, RAFT addition becomes less favourable.[21] The corresponding RAFT polymerization is often referred to as macromolecular design by interchange of xanthates (MADIX), due to historical reasons of its discovery.[22,23]

As a result of the low S=C double-bond character of xanthates, microstructural control ($Đ$ < 1.5) can typically only be achieved by employing so-called less activated monomers (LAMs) such as ethylene and vinyl acetate. These monomers typically contain a saturated carbon or an oxygen/nitrogen electron pair adjacent to the vinyl group, resulting in more reactive radicals with respect to RAFT addition ($C_{\mathrm{tr}(,0)}$ > 10).[17,19,21,24–29] Other more active RAFT agents such as dithioesters and trithiocarbonates (Fig. 1c) lead to the formation of INT radicals considerably more stable than the radicals formed by RAFT fragmentation, resulting in an undesired lowering of the polymerization rate. With xanthates, the increased stability of R_0X, due to the delocalizable lone electron pairs, and the sufficient destabilization of the radical centre of the corresponding INT species allow simultaneously lowering the RAFT addition reactivity and realizing a more favourable RAFT fragmentation as compared to other types of RAFT agents.

On the other hand, bulk or solution MADIX of so-called more activated monomers (MAMs), such as (meth)acrylates and styrenics which possess vinyl groups conjugated by a carbonyl group or an aromatic ring, can typically not be conducted easily with good control over chain length. Research in this area is thus still challenging as the radicals are less reactive for RAFT addition and the less active xanthate may not actively participate during polymerization ($C_{\mathrm{tr}(,0)} \ll 10$). Rate retardation and inhibition are also typically absent so that a degenerative RAFT mechanism (Fig. 1b) can be often assumed, strongly simplifying the overall kinetic description.[5,7,30–34]

A crucial design parameter, as for every RAFT polymerization,[15,16,35] is thus the selection of appropriate MADIX agent substituents as this determines $C_{\mathrm{tr}(,0)}$. For MADIX of MAMs, several kinetic studies have been performed with styrene as the monomer.[7,17,19,25,32,34,36,37] For example, Adamy *et al.*[7] investigated the influence of the chemical structure of the initial RAFT agent for MADIX of styrene in toluene and reported that with (*O*-ethyl xanthate)-2-ethyl propionate (OEXEP) as the initial RAFT agent, a $Đ$ close to 2 (X_{m} = 20%) can merely be obtained. In contrast, by increasing the electron-withdrawing capacity of the Z group by incorporation of fluorinated groups at β-position to the oxygen atom, as for instance in (*O*-2,2,2-trifluoro ethyl xanthate)-2-ethyl propionate (OtFOX), a lower but

still high $Đ$ of 1.6 can be achieved (X_m > 20%), in agreement with an earlier experimental study by Destarac *et al.*[36] The latter observation was attributed to an increased reactivity of the S=C bond due to the decreased availability of the oxygen lone pair to conjugate with the thiocarbonyl group. This also followed from a comparison of the $C_{tr,0}$ (eqn (4)) values.[7,37]

It should be stressed that solely focusing on $C_{tr,0}$ is very likely insufficient to unequivocally predict the success of a MADIX process. For example, for *O*-ethyl-*S*-[(2-phenyl)prop-2-yl] dithiocarbonate, Destarac *et al.*[37] determined a rather high $C_{tr,0}$ of 3.8 at 110 °C for styrene, which has been related to the higher stability of the leaving tertiary benzylic radical as compared to the styryl radical. Despite this promising $C_{tr,0}$ value, only polystyrene with a high $Đ$ (≈2) could be obtained (X_m > 80%), which has been attributed to a lower C_{tr} (eqn (6)) value close to 1, as assessed using Müller's equation.[38] In several studies[7,32,34] C_{tr} has, however, been taken to be equal to $C_{tr,0}$, which can thus be expected to be an oversimplification of the description of the RAFT/MADIX polymerization kinetics.

For MADIX, the main focus has been on the determination of $C_{tr,0}$. In general, the applicability of the methods used to determine $C_{tr,0}$ strongly depends on the validity of their model assumptions.[20] Under the common assumption of a degenerative RAFT mechanism (sufficiently fast RAFT fragmentation), the Mayo[39] and CLD methods[40] have been mostly applied.[20] Alternatively, Moad and coworkers[15,16,35] demonstrated that $C_{tr,0}$ can be evaluated from the slope of a plot of ln[R_0X] *vs.* ln [M], at least in case the RAFT exchange with R_0 radicals ($k_{-tr,0}$; Fig. 1b) can be assumed to be negligible.

Unfortunately, for C_{tr}, as recently highlighted by Derboven *et al.*,[20] no reliable (analytic) method exists which can be safely used for a broad range of conditions and RAFT reactivities, in particular in case $C_{tr,0}$ strongly differs from C_{tr}. Only very recently, a novel method based on the measured dispersities has been proposed to jointly determine $C_{tr,0}$ and C_{tr} in a single experimental run.[8] This method requires a rather controlled degenerative RAFT polymerization with sufficiently low dispersities (<1.3), which are typically not encountered in MADIX. Currently, for MADIX, C_{tr} could only be assessed using size exclusion chromatography (SEC) data. In particular, Smulders *et al.*[30] applied the method of Goto[41–43] to assess C_{tr} during chain extension of dormant polystyrene in toluene with *n*-butyl acrylate and OEXEP as the RAFT agent. A C_{tr} value of 1.04 (60 °C) resulted, which is rather approximate, taking into account the overlap between the SEC traces for the dormant polystyrene and the obtained block copolymer at the low molar mass region of the SEC trace.

Despite the somewhat restricted mediating capacities of xanthates under bulk and solution conditions and the difficulty of mapping the impact of the chemical structure on the RAFT transfer reactivities, MADIX remains of particular interest for all monomer types. This becomes clearer by highlighting that MADIX can be successfully conducted in water-based media (*e.g.* (mini)emulsion), without issues related to colloidal instability.[5,7,44–47] A key feature is the xanthate surface activity, which allows the synthesis of covalently linked core–shell nanoparticles with typically styrene as the core.[30,33,48] Be that as it may, exit/entry and even re-entry phenomena can disturb the desired growth so that the identification of the most suited conditions is non-trivial.[49–52]

To facilitate the identification of the suited MADIX/RDRP bulk, solution and emulsion conditions, model-based design has been shown to be a powerful and indispensable tool, as it minimizes the need for long trial and error based experimental approaches with a full mapping of the relationship between process parameters and RDRP characteristics.[11,53–60] A prerequisite for a model-based design are accurate intrinsic rate coefficients. As explained above, for MADIX, only a limited number of exchange kinetic parameters are available.[7,15,16,20,36,61] Hence, further research on the determination of MADIX-specific kinetic parameters is still needed to fully exploit its potential, in particular in view of emulsion applications.

In the present work, a detailed combined experimental and simulation study is presented of bulk MADIX of styrene at 70 °C with OEXEP as the initial RAFT agent and AIBN as the conventional radical initiator. Average characteristics are simulated deterministically and detailed microstructural properties are obtained through parallel stochastic kinetic Monte Carlo (*k*MC) simulations. Dedicated regression analysis is applied to determine both $C_{tr,0}$ and C_{tr}, considering an extensive set of experimental data, including data on RAFT agent conversion, $Đ$, and EGF. The EGF data are reliably measured by consecutively performing dialysis to remove residual OEXEP and elemental analysis to determine the sulphur and nitrogen content for the polymer samples. It should be noted that, in general, EGF determination is challenging,[62] especially for high molar mass polymers for which the accuracy of techniques such as proton nuclear magnetic resonance (^{1}H-NMR),[63–68] ultraviolet (UV) spectroscopy,[69,70] matrix-assisted laser desorption/ionization time-of-flight,[61,62,71,72] and even elemental analysis[73] is limited. The modelling tools are used to understand better the MADIX mechanism and to visualize – for the first time – the monomer sequences along individual chains during chain extension with (i) styrene or (ii) *n*-butyl acrylate (*n*BuA).

Experimental

Materials

Styrene (Sty, monomer (M), ≥99%, Sigma-Aldrich) was passed through a column filled with basic aluminium oxide (Sigma-Aldrich) to remove the stabilizer (4-*tert*-butylcatechol). 2,2-Azobis(2-methyl-propionitrile) (AIBN, a conventional radical initiator (I_2), ≥98.0%, Sigma-Aldrich) was purified twice by recrystallization from methanol (≥99.6%, Sigma-Aldrich) and stored afterwards at −18 °C. *n*-Decane (≥99%; internal standard), tetrahydrofuran (THF, ≥99%), dichloromethane (DCM, ≥99%), ethanol, diethyl ether (≥98%), pentane (98%), ethyl 2-bromopropionate (99%), and potassium *O*-ethyl dithiocarbonate (96%) were purchased from Sigma-Aldrich and used as

received. Ethanol (>99.8%) was purchased from Chem-Lab and used as received as well. Distilled water was further purified through a Millipore Milli-Q Plus system. Cellulose ester dialysis membranes with a molar mass cut-off between 5×10^2 and 10^3 g mol^{-1} were obtained from Spectrum Labs and soaked in deionized water and subsequently rinsed thoroughly prior to usage in order to remove the sodium azide preservative agent.

MADIX synthesis procedures

A typical isothermal MADIX homopolymerization was performed as follows (entry 7 in Table S1 in ESI† which presents an overview of all the initial homopolymerization conditions). A mixture of styrene (35 mL), OEXEP (0.697 g; synthesis procedure in section S2 of the ESI†), AIBN (0.050 g), and *n*-decane (2 mL) was added to a 100 mL two-neck glass flask containing a magnetic stirrer bar. A stopcock was attached to one neck and a rubber septum to the other. The solution was degassed by three freeze–pump–thaw cycles after which an argon environment was established. The flask was immersed in a preheated oil bath at the desired polymerization temperature (70 °C) and constantly stirred at 300 rpm. This temperature has been selected in view of a future extension to MADIX emulsion polymerization.[33,74,75] Moreover, the self-initiation of styrene is suppressed, simplifying the overall kinetic description.[76] Temperature control was possible through *in situ* measurements *via* a thermocouple inserted in the rubber septum. Samples (1.5 mL) were withdrawn from the reaction flask at distinct, predefined reaction times, using 2 mL degassed syringes with stainless-steel needles, and immediately quenched in liquid nitrogen.

For the MADIX chain extensions (Table S2 in the ESI† for an overview of all the conditions), an analogous synthesis procedure as that for the homopolymerizations was used. The necessary polystyrene reactant (RX) was first synthesized by performing a homopolymerization experiment on a larger scale (100 mL styrene; entry 3 in Table S1 in the ESI†). Importantly, the polystyrene obtained during this first synthesis step was purified by means of dialysis in order to remove unreacted OEXEP (R_0X). The samples were loaded into the dialysis tubing and placed in toluene (volume ≈50 times the sample volume). The dialysis was run for 96 h at room temperature while renewing the toluene dialysate five times at approximately 8, 24, 48, 56, and 72 h. Afterwards, the samples were extracted from the membrane and toluene was removed by means of rotary evaporation (80 °C; 250 mbar; 2 h) and freeze-drying (~10^{-2} mbar; 1 h). As explained in section S5 of the ESI,† the molar amount of RX in the purified samples (n_{RX}) was determined using:

$$n_{RX} = \frac{m_{PS}}{M_n}\mathrm{EGF} \quad (7)$$

in which m_{PS} is the polystyrene mass and M_n the number average molar mass.

Both the homopolymerization and chain extension experiments were performed in duplicate and the reproducibility was always identified to be very high.

The elemental analysis samples for the EGF measurements of the homopolymerizations were obtained by a similar dialysis procedure (toluene volume ≈200 times the sample volume; dialysis time 48 h; renewal of dialysate at approximately 3, 18, 22, 27, 38, and 41 h). The successful removal of R_0X could be confirmed by ^{1}H NMR and size exclusion chromatography (SEC) analyses (see the Results and discussion section).

Analytic techniques

Monomer and RAFT agent conversions (X_m and X_{R0X}) were determined by gas chromatography (GC). GC analysis was carried out using a trace-GC ultra-gas chromatograph equipped with an AS3000 auto sampler, a flame ionization detector (FID), and a CP WAX 52 CB 30 m capillary column. Helium (flow rate: 1.5 mL min^{-1}) was used as a carrier gas and the following stepwise temperature programme was applied: (i) 50 °C for 4 min; (ii) heating ramp of 20 °C min^{-1} until 300 °C; (iii) 300 °C for 5 min. DCM was used as a solvent to prepare the samples and *n*-decane was present in the reaction mixture as an internal standard. Data acquisition and processing were performed using Chrom-Card Trace-Focus GC software. The GC results were successfully confirmed by ^{1}H NMR (Fig. S2 in the ESI†). The spectra were recorded at 400 MHz and ambient temperature with $CDCl_3$ as a solvent, using a Bruker Avance II spectrometer equipped with a Broadband Observe (BBO) probe.

GC analysis and ^{1}H NMR were also applied to investigate the efficiency of the OEXEP synthesis (molar purity: 97 ± 1%; Fig. S1 in the ESI†). Only a significant amount of ethyl 2-bromopropionate remained (±3%) but no other impurities or side products could be detected.

Number/mass average molar mass ($M_{n/m}$) and dispersity ($Đ$) were measured *via* SEC by injecting polymer samples diluted with THF. A PL-GPC50 Plus instrument equipped with a PL-AS RT auto sampler and a refractive index (RI) detector, one Resipore 50 × 7.5 mm guard column and two Resipore 300 × 7.5 mm columns in series were used. The flow rate was 1 mL min^{-1} and the analysis temperature was 30 °C. Calibration for homopolymerization and chain extension of styrene was performed with narrow polystyrene standards (Medium EasiVials kit, Agilent Technologies), ranging from 1.62×10^2 to 4.83×10^5 g mol^{-1}. Data acquisition and processing were performed using the PL Cirrus GPC/SEC software.

EGF values of polymer samples after dialysis, hence after removal of R_0X, were determined by means of elemental analysis, using a Flash 2000 organic elemental analyser (Thermo Scientific) equipped with a thermal conductivity detector (TCD). Calibration was performed with a 2,5-bis(5-*tert*-butylbenzoxazol-2-yl) thiophene (BBOT) standard.

The EGF value, which reflects the amount of X end-groups for the total number of chains, follows from:

$$\mathrm{EGF} = \frac{n(\mathrm{X})}{0.5[n(\mathrm{I}) + n(\mathrm{R_0}) + n(\mathrm{X})]} \quad (8)$$

in which n(A) (A = R_0, X, and I) is the molar amount of A groups in the polystyrene sample (for calculations see section

S7 of the ESI†), neglecting end-groups originating from chain transfer of macroradicals to monomer as verified in section S9 of the ESI.† The factor 0.5 reflects that all chains possess two chain ends of one of the three considered end-group types in the denominator of eqn (8) (see also Fig. 3; top right).

Kinetic modelling and regression analysis

MADIX of styrene and its chain extension are modelled with both a fast deterministic and a detailed stochastic method, assuming a degenerative RAFT exchange mechanism (Fig. 1b). This mechanism can be used taking into account the fact that the RAFT fragmentation can be expected to be fast and the RAFT addition slow.[7,19,21,32,77] As shown by De Rybel *et al.*,[11] for low RAFT addition rate coefficients ($<10^{2.5}$ L mol^{-1} s^{-1}) with styrene, even an extremely low RAFT fragmentation rate coefficient of 10^{-2} s^{-1} still results in no observable rate retardation or RAFT-cross-termination, further supporting the use of a degenerative mechanism.

For the deterministic modelling, the so-called extended method of moments[78–82] is used, allowing the simulation of the evolution of the monomer and R_0X conversion and average polymer characteristics such as the number and mass average chain length ($x_{n/m}$), $Đ$, and EGF. Since this method is very fast it facilitates the estimation of the RAFT exchange parameters (*cf.* eqn (1)–(3)). Moreover, population weighted or thus averaged apparent termination rate coefficients are considered. For the calculation of these averages, the macroradical CLD can be approximated by the Flory–Schulz distribution (see below). For the stochastic modelling, the kinetic Monte Carlo technique (*k*MC) is employed, following the basic algorithm of Gillespie[83] extended as previously described to map the polymer microstructure with a high level of detail.[57,84,85] More details of this approach are provided in section S10 of the ESI.† Importantly, it has been verified that the simulated average characteristics of both computational methods converge (see Fig. S6 in the ESI†).

The transfer rate coefficients $k_{tr,0}$ and k_{tr}, allowing the calculation of the corresponding degenerative RAFT coefficients $C_{tr,0}$ and C_{tr} (eqn (4)–(6)), have been estimated based on an extensive set of polymerization data, using the deterministic kinetic model and the Levenberg–Marquardt algorithm (ODRPACK v2.01).[86] For a detailed description of the regression analysis procedure, the reader is referred to earlier work.[87,88] The transfer coefficient $k_{-tr,0}$ could be neglected based on preliminary simulations (see section S12 of the ESI†), indicating that reaction of R_0 radicals with monomer is strongly preferred over reaction with R_0X. Similarly, exchange between conventional initiator radicals (I) and R_0X is kinetically insignificant as the addition of monomer to I is sufficiently fast (see section S13 of the ESI†).

An overview of the reactions considered in the degenerative RAFT kinetic model and their associated kinetic parameters is provided in Table S3 (styrene) and Table S6 (*n*BuA) in the ESI.† For the chain extension with *n*BuA, for simplicity and taking into account the expected limited impact, a possible penultimate monomer unit effect is ignored. Specifically for termination, apparent rate coefficients are considered to account for diffusional limitations, according to the well-established RAFT-chain length dependent-termination (RAFT-CLD-T) technique. These coefficients are chain length and X_m dependent and their model parameters are listed in section S15 of the ESI.† For the "block copolymer radicals", an averaging according to the overall copolymer composition is performed, as explained in section S14 of the ESI† and in agreement with a previous kinetic modelling study.[89–99] Diffusional limitations on the other reaction steps are neglected, based on the literature data,[80,92,100,101] taking into account the fact that the maximal X_m is limited and the RAFT addition rate coefficients are relatively low.

Results and discussion

In this section, attention is first paid to EGF determination by combining dialysis and elemental analysis, with AIBN/OEXEP as the MADIX initiation system and styrene as the monomer. Next, our focus is on the validity of the kinetic model assumptions to ensure a reliable *in silico* interpretation of the MADIX characteristics and mechanism. Finally, a detailed kinetic analysis of both the MADIX homopolymerization and the chain extension with fresh styrene or *n*BuA, starting from isolated (dormant) polystyrene, is performed. The monomer sequences and end-groups of each chain of a representative (co)polymer sample are visualized, considering the $C_{tr(,0)}$ values as determined based on tuning to experimental data.

Validation of EGF determination

As indicated above, it is not straightforward to retrieve reliable EGF data for RDRP processes. An additional complication in the present work is the rather slow OEXEP (R_0X) consumption, resulting in a significant amount of unreacted OEXEP during the homopolymerization with styrene, making elemental analysis without prior purification challenging. Moreover, to facilitate chain extension and to accurately estimate k_{tr} (or C_{tr}), reactions with R_0X need to become kinetically insignificant and, hence, unreacted OEXEP needs to be removed.

For R_0X removal, as shown in section S16 of the ESI,† conventional precipitation is not recommended as SEC analysis shows that a significant amount of oligomeric species is also removed along with R_0X. On the other hand, in case dialysis is performed a successful R_0X removal is realized as shown in Fig. 2. For a typical homopolymerization (entry 1 in Table S1 in the ESI;† X_m = 33%), dialysis ensures a complete removal of the initial RAFT agent (Fig. 2; top ^{1}H-NMR data) without altering the polymer part of the SEC trace (Fig. 2; bottom). After dialysis, elemental analysis of the purified polystyrene samples is performed to determine the mass fractions of carbon, hydrogen, nitrogen, and sulphur. The associated chromatogram for the purified product in Fig. 2 is depicted in Fig. 3. As the polymer is linear and consists of styrene units, carbon and hydrogen generate the largest peaks. In contrast, nitrogen and

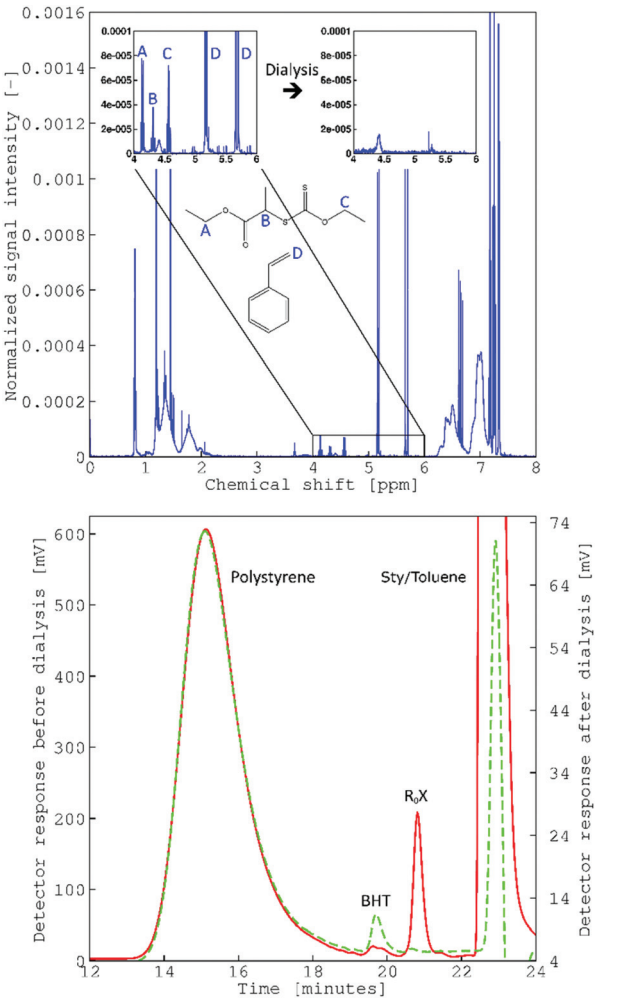

Fig. 2 Verification of the reliability of dialysis to remove the initial RAFT agent (OEXEP); top: ^{1}H-NMR spectrum before (the main spectrum and in detail, top left) and after (only in detail, top right) dialysis with the assignment of relevant peaks for OEXEP and styrene; bottom: SEC trace before (solid red line) and after (dashed green line) dialysis; BHT: butylated hydroxytoluene (THF (SEC eluent) stabilizer); M_n (before) = 6.1 × 10^3 g mol^{-1}, M_m (before) = 12.2 × 10^3 g mol^{-1}, and $Đ$ (before) = 2.0; M_n (after) = 5.9 × 10^3 g mol^{-1}, M_m (after) = 12.2 × 10^3, and $Đ$ (after) = 2.1; entry 1 in Table S1 in the ESI,† X_m = 33%.

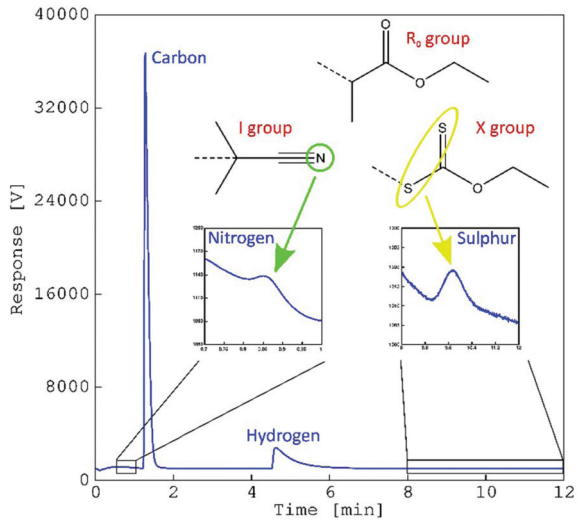

Fig. 3 Typical elemental analysis chromatogram for MADIX homopolymerization of styrene (entry 1 in Table S1 in the ESI;† X_m = 33%; the related purified SEC trace in Fig. 2), allowing EGF measurement according to eqn (8). Reliable assumption of linear chains with, as end-groups, either R_0 and X; I and X; I and I; R_0 and R_0; or R_0 and I; negligible contribution of chain transfer to monomer (see section S9 of the ESI†) and R_0R_0 formation (see section S8 of the ESI†).

sulphur are only present in the end-groups (Fig. 3; top right) and, hence, result only in minor peaks. This implies that the most reliable EGF data are only obtainable at lower TCLs at which the relative importance of the end-groups is higher.

Validation of kinetic modelling assumptions

For a fast simulation of the MADIX process, as explained above, the deterministic extended method of moments is applied. This method only aims at the description of the temporal evolution of X_m and the average CLD characteristics but takes into account (apparent) chain length dependencies. This is done by the calculation of averaged apparent termination rate coefficients while assessing the macroradical concentrations using a predetermined distribution. For example, the zeroth order averaged apparent termination (by recombination) rate coefficient ($\langle k_{tc,app}\rangle$), as needed to integrate the moment equations, is defined by:

$$k_{tc,app} = \frac{\sum_{i=1}^{\infty}\sum_{j=1}^{\infty} k_{tc,app}^{i,j}(1+\delta_{ij})[R_i][R_j]}{\left(\sum_{i=1}^{\infty}[R_i]\right)^2} \quad (9)$$

in which $k_{tc,app}^{i,j}$ is the apparent termination (by recombination) rate coefficient between macroradicals with a chain length i and j (values: section S14 of the ESI†), δ_{ij} is the Kronecker Delta function, and $[R_i]$ and $[R_j]$ are the corresponding concentrations. In the present work, these individual concentrations are assumed to follow a Flory–Schulz distribution:

$$f_n(i) = \frac{[R_i]}{\sum_{i=1}^{\infty}[R_i]} = \frac{1}{x_{n,r}}\exp\left(-\frac{i}{x_{n,r}}\right) \quad (10)$$

with $f_n(i)$ being the number fraction of macroradicals with a chain length i and $x_{n,r}$ the associated number average chain length.

For homopolymerization the use of the Flory–Schulz distribution is valid, as shown in Fig. 4 (entry 3 in Table S2 in the ESI†) focusing on the simulation of X_m (0–8 h; top left) and in Fig. S6 of the ESI† focusing on the simulation of the average CLD characteristics. A perfect match is obtained between the results for the (approximate) deterministic simulations (green full lines) and the *k*MC simulations (red dotted lines) which fully take into account chain length dependencies. The validity of eqn (10) is also reflected in the simulated number macro-

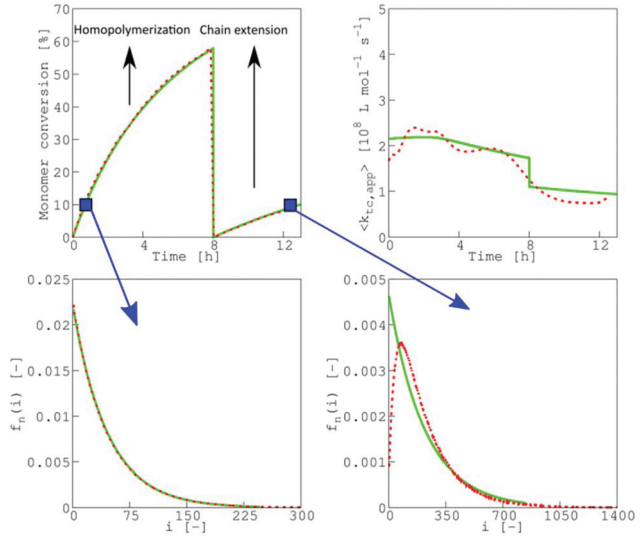

Fig. 4 Comparison of the main simulation results for MADIX homopolymerization and chain extension with fresh styrene obtained with the deterministic extended method of moments, assuming a Flory–Schulz macroradical CLD (eqn (10)) (full green lines) and with a *k*MC model explicitly accounting for all chain length dependencies (dotted red lines). Monomer conversion (top left) and zeroth order average apparent rate coefficient (eqn (9); top right); homopolymerization conditions: 0–8 h (entry 3, Table S1 in the ESI†) and chain extension 8–13 h (entry 3, Table S2 in the ESI†); bottom left: macroradical CLD at X_m = 10% for MADIX homopolymerization and bottom right: for chain extension at the same conversion; dotted line in top right: for a single *k*MC run.

radical CLDs (*e.g.* Fig. 4 bottom left; X_m = 10%), which also match, leading to similar variations for $\langle k_{tc,app} \rangle$ (Fig. 4 top right; eqn (9)). This result cannot be generalized to a typical RAFT polymerization[102] but is specific for the selected MADIX process in which Flory–Schulz character is obtained for the control over chain length.

Also for the chain extensions the deterministic method can be used for the reliable calculation of the average MADIX characteristics. Despite a mismatch at the low chain lengths for the macroradical CLDs (*e.g.* bottom right in Fig. 4; X_m = 10%; entry 3 in Table S2 in the ESI†), the monomer conversions and average CLD characteristics are still identical for the deterministic and *k*MC simulations, as shown in Fig. 4 (top left; X_m evolution for 8–13 h) and as shown in Fig. S6 in the ESI† (average CLD characteristics). Note that the chain extended macroradicals are not Schulz–Flory distributed. To obtain Flory–Schulz behavior both segments should be of similar lengths, *e.g.* short original segments should be extended again with short ones, which is statically unlikely. Instead of a Flory–Schulz distribution a Gamma like distribution results (Fig. 4 bottom right).[103]

Microstructural control for MADIX styrene homopolymerization

To obtain a better understanding of the homopolymerization kinetics, a systematic experimental study has been conducted under isothermal conditions (70 °C), including a variation of all initial batch concentrations. In Fig. 5 and 7, the experimental data on X_m, R_0X conversion (X_{R0X}), number and mass average chain length (x_n and x_m), EGF, and $Đ$ are provided under several initial conditions (entries 1–6 in Table S1 of the ESI†) along with the corresponding simulation results (parameters Table S3 in the ESI†).

For all data, excellent agreement between the experimental and simulated data is obtained. Similarly, for the additional data in Fig. S10 in the ESI (entry 7 in Table S1†), the experimental data are well described.

Investigation of Fig. 5 allows concluding that an increase of the initial I_2 concentration (lower $[R_0X]_0/[I_2]_0$) leads to an increase of both X_m and X_{R0X} (Fig. 5; left) while having a limited effect on the average chain length characteristics x_n, x_m, and $Đ$ (Fig. 5; middle and right). At all times, high x_n values, roughly 10% higher than the TCL, are obtained with constant $Đ$ values close to 2. The EGF data (Fig. 5; right) indicate a relatively high livingness (>80%), which is also time independent. Greater EGF values are obtained for decreasing I_2 amounts, further highlighting the relevance of the optimization of $[R_0X]_0/[I_2]_0$. On the other hand, as can be derived from Fig. 7, an increase of TCL ($[M]_0/[R_0X]_0$) at a given $[I_2]_0$ (4×10^{-3} mol L^{-1}) has no notable influence on X_m and X_{R0X} (Fig. 7; left) while it results in a reduction of x_n and x_m (Fig. 7; middle). The chain length characteristics again remain constant throughout the MADIX. A lower livingness is obtained at higher TCLs (Fig. 7; right) whereas $Đ$ remains again constant around a value of 2. Hence, on an overall basis, the effect of TCL is relatively restricted aside from its natural influence on the average chain lengths.

Further model analysis shows that for the studied MADIX homopolymerization RAFT exchange involving macrospecies (k_{tr}) is negligible. As illustrated in section S18 in the ESI,† identical simulation results are obtained for a k_{tr} (eqn (3)) value equal to 0 L mol^{-1} s^{-1} and if k_{tr} is taken to be equal to ten times $k_{tr,0}$. From this, it can be concluded that the rate of exchange between macrospecies is too low to significantly affect the concentration of macroradicals. The latter are only involved in propagation, termination or in RAFT exchange with R_0X. Since the rate of re-initiation is, in addition, significantly higher than the rate of exchange of R_0 radicals and dormant macrospecies, the latter exchange, characterized by $k_{-tr,0}$, is also kinetically insignificant as shown in section S12 of the ESI.† The homopolymerization data in Fig. 5, 7, and S10 in the ESI† are therefore only affected by a single RAFT transfer parameter, *i.e.* $C_{tr,0}$ (eqn (4)). Hence, for the current MADIX system, several of the reactions/exchanges of Fig. 1 are kinetically insignificant and the reaction scheme can be represented by the one in Fig. 6. It is clear from the reduced scheme that the formation of the dormant species can be formally compared to chain transfer with a conventional chain transfer agent such as 1-butanethiol, although with a single transfer of X instead of H.[104] Note that in this context transfer is thus defined as a consecutive addition and fragmentation to the "right".

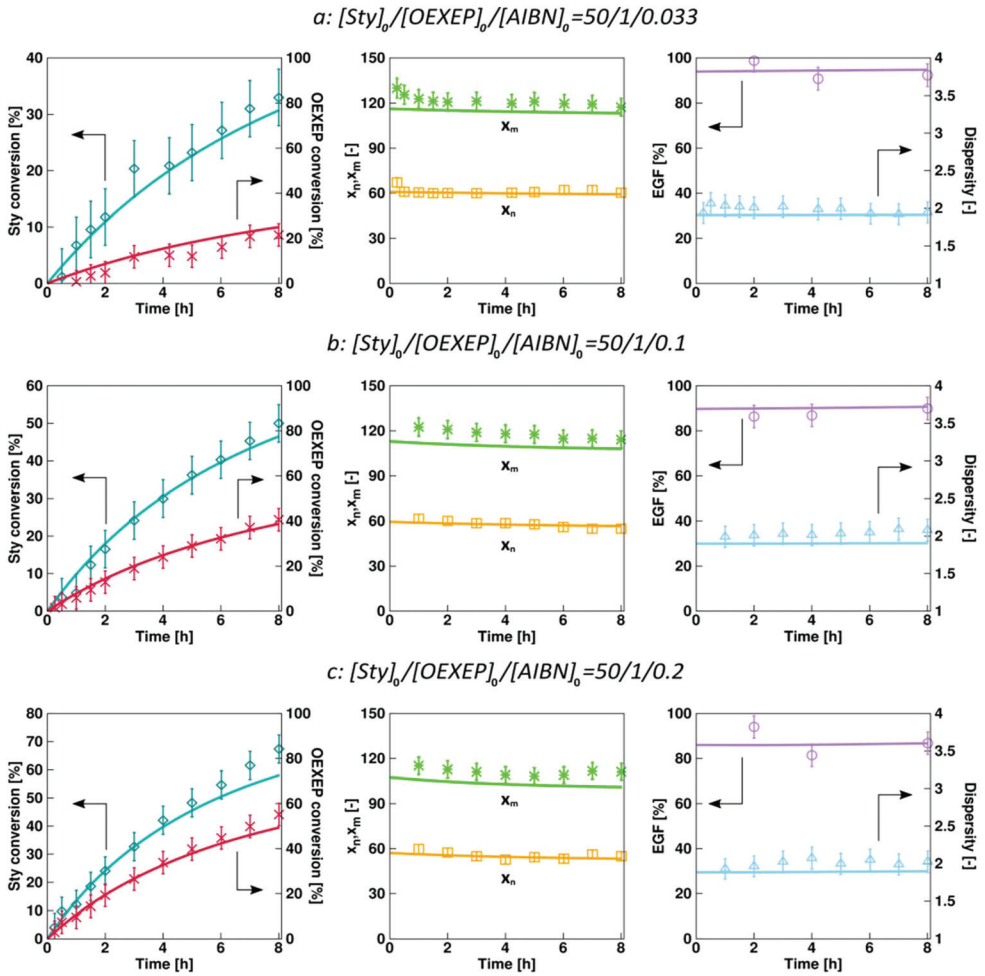

Fig. 5 Comparison of simulation and experimental data for a variation of $[OEXEP]_0/[AIBN]_0$ for MADIX homopolymerization of styrene at 70 °C with AIBN and OEXEP; monomer conversion (X_m, dark blue), R_0X conversion (X_{R0X}, red), number-average chain length (x_n, orange), mass-average chain length (x_m, green), dispersity ($Đ$, purple), and end-group functionality (EGF, light blue) as a function of time; lines correspond to calculated values with rate coefficients given in Table S3 in the ESI† and accounting for diffusional limitations (parameters in Table S4); entries 1–3 in Table S1 in the ESI;† simulated output with the deterministic method.

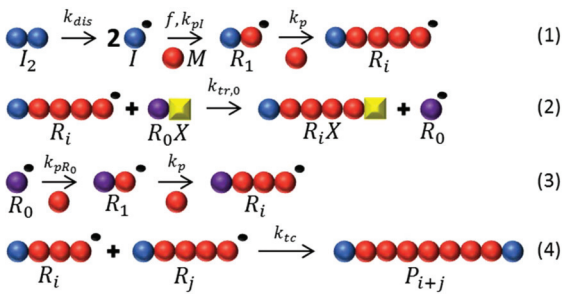

Fig. 6 Simplified reaction scheme for MADIX homopolymerization of styrene with OEXEP as the initial RAFT agent, starting from the general RAFT polymerization reaction scheme (Fig. 1). Other steps of Fig. 1 are kinetically insignificant.

The $C_{tr,0}$ value obtained through multi-response regression analysis (0.80 ± 0.02) is larger than the value obtained following the previously developed methods of Mayo (0.71 ± 0.02; section S19 of the ESI†) and Moad (0.69 ± 0.04; section S19 of the ESI†),[7,15,16,20,35] which focus only on x_n and $X_{M/R0X}$ data, respectively. As demonstrated in Fig. 8 (entry 4 in Table S1 in the ESI†), the increased $C_{tr,0}$ value results in a good prediction of all average MADIX characteristics, whereas the use of the lower values obtained from the literature methods lack the capability of accurately predicting experimental x_n and x_m data. With the two literature methods, too high average chain lengths are simulated at all times. For the Mayo method, this inaccurate reflection of the x_n data seems at first sight surprising as the $C_{tr,0}$ is determined based on this response alone. As explained in section S20 in the ESI,† the Mayo method is only fully accurate if the theoretical kinetic chain length can be represented by the experimentally accessible x_n, which is only true in the absence of dead chains formed by termination by recombination. This highlights the relevance of multi-response regression analysis using the detailed modelling strategy in the present work.

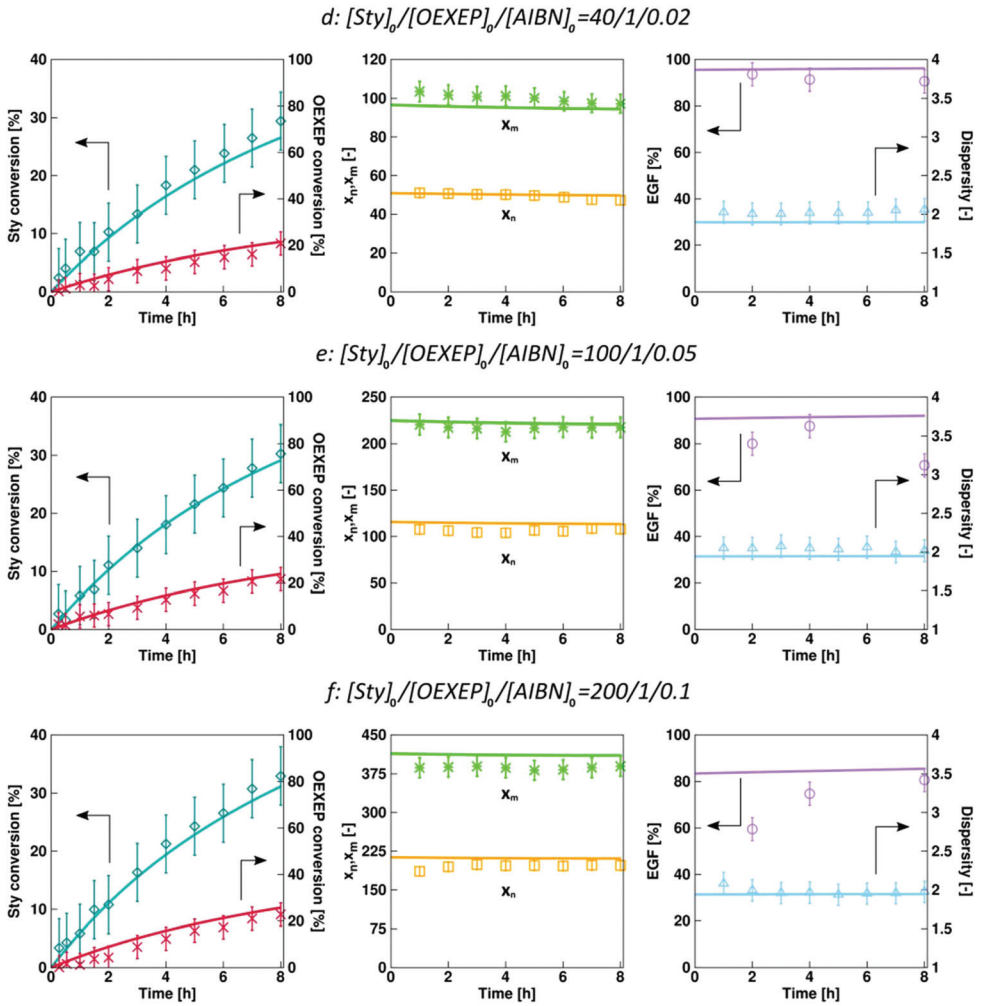

Fig. 7 Comparison of simulated and experimental data for a variation of TCL ($[M]_0/[OEXEP]_0$) at a given $[I_2]_0$ (4×10^{-3} mol L^{-1}) for MADIX homopolymerization of styrene at 70 °C with AIBN and OEXEP; monomer conversion (X_m, dark blue), R_0X conversion (X_{R0X}, red), number-average chain length (x_n, orange), mass-average chain length (x_m, green), dispersity ($Đ$, purple), and end-group functionality (EGF, light blue) as a function of time; lines correspond to calculated values with rate coefficients given in Table S3 in the ESI† and accounting for diffusional limitations (parameters in Table S4†); entries 4–6 in Table S1 in the ESI;† simulated output with the deterministic method.

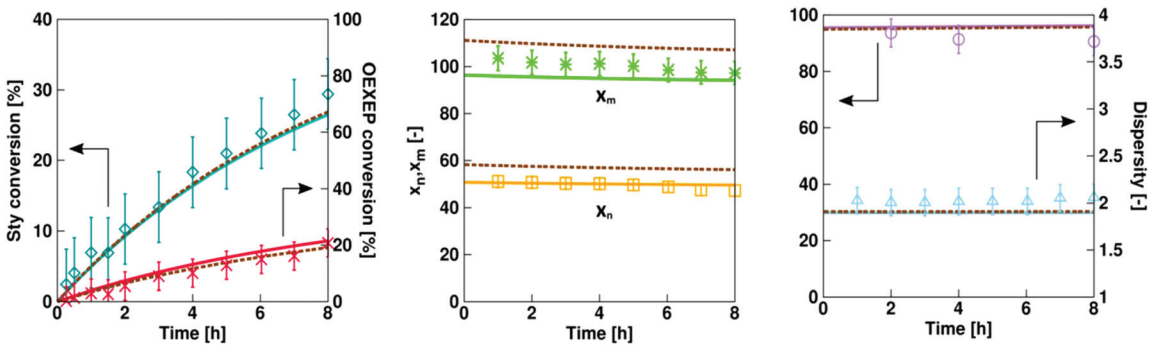

Fig. 8 Relevance of applying multi-response regression analysis to all average MADIX characteristics to estimate $C_{tr,0}$ compared to previously developed methods of Mayo[39] and Moad[15,16,35] which focus only on, respectively, x_n and $X_{M/R0X}$ data; entry 4 in Table S1 of the ESI† with full lines corresponding to the results with the multi-response regression analysis ($C_{tr,0}$ = 0.80; this work) and the brown dashed lines ($C_{tr,0}$ = 0.69) after application of the literature methods (section S19 of the ESI†).

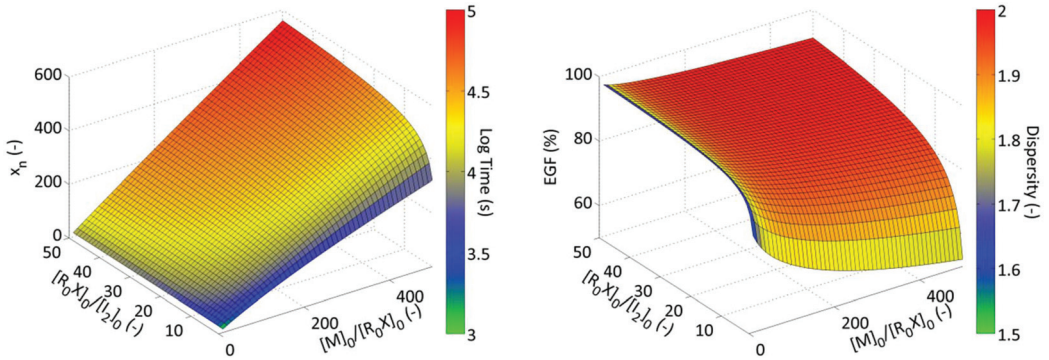

Fig. 9 Number-average chain length (x_n, left) and end-group functionality (EGF, right) as a function of $[R_0X]_0/[I_2]_0$ (ranging from 1 to 50) and $[M]_0/[R_0X]_0$ (ranging from 10 to 500) and the corresponding polymerization time (left; color) and dispersity (right; colour); simulated data have been achieved by means of the parameters given in Table S3† with R_0X = (*O*-ethyl xanthate)-2-ethyl propionate, M = Sty, and I_2 = AIBN; 70 °C; X_m = 20%.

Another advantage of the modelling strategy is the possibility to map the MADIX characteristics over a broad operating window, as shown in Fig. 9 focusing on the simultaneous prediction of the reaction time, x_n, EGF, and $Đ$ at a fixed X_m of 20%, with $[M]_0/[R_0X]_0$ and $[R_0X]_0/[I_2]_0$ values ranging, respectively, from 10 to 500 and from 1 to 50. As shown in Fig. S14 in the ESI† for every condition in Fig. 9 the R_0X conversion (X_{R0X}) is equal to *ca.* 16%, again highlighting the low reactivity of xanthates towards styryl macroradicals and that the exchange with the initial RAFT agent is dominant in the selected MADIX homopolymerization.

Since R_0X acts as a conventional CTA, as indicated above, it follows from Fig. 9 (left) that x_n can be controlled by varying its initial concentration. In agreement with the results in Fig. 5, an increase of $[R_0X]_0/[I_2]_0$ leads to higher EGF values (Fig. 9; right) but also to higher reaction times (Fig. 9; left). Additionally, high $Đ$ (close to 2; Fig. 9 right) values are obtained under all conditions, except at very low $[M]_0/[R_0X]_0$ for which $Đ$ is reduced to a value close to 1.5. As shown in Table 1, the coefficients of variation of both the dormant and dead polymer CLD (CV(RX) and CV(P)), which are defined as the ratio of the standard deviations (that are related to the dispersities) to the number average chain lengths, are lower for decreasing $[M]_0/[R_0X]_0$, explaining the aforementioned trend for the (overall) $Đ$. Note that the dormant population is the key contributor to $Đ$, as high EGF values always result. As explained above (Fig. 6), the latter population is formed by a single RAFT exchange. Hence, by adding more R_0X for a given initial M amount, a more rapid chain transfer takes place. This leads to a lowering of $Đ$, eventually to a value of 1.5.

Table 1 $Đ$, EGF, and x_n for two different $[M]_0/[R_0X]_0$ in Fig. 9 (X_m = 20%) with the coefficient of variation CV (ratio of CLD standard deviation to mean value (x_n)), differentiating between dormant (RX) and dead (P) polymers

$[M]_0/[R_0X]_0/[I_2]_0$	$Đ$	EGF	x_n	CV_{tot}	CV(RX)	CV(P)
10/1/0.2	1.66	0.91	14.18	0.81	0.95	0.68
50/1/0.2	1.88	0.86	55.78	0.94	0.99	0.71

In addition, the detailed *k*MC simulations allow explicitly visualizing the microstructure of individual chains, including a differentiation according to the end-groups as defined in Fig. 3 (top right). For instance, for entry 3 in Table S1 in the ESI,† Fig. 10 (top) shows the lengths and end-groups of *ca.* 1500 randomly selected chains out of a *k*MC simulation system consisting of *ca.* 10^8 chains, at t = 8 h (X_m = 60%).

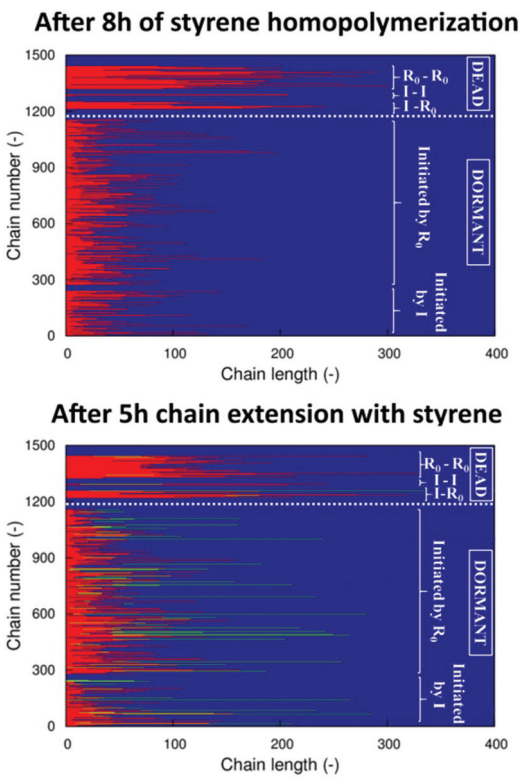

Fig. 10 Visualization of the detailed microstructure of *ca.* 1500 individual chains for homopolymerization of styrene (top, after 8 h, red, x_n = 51) and its subsequent chain extension with fresh styrene (bottom, after 5 h; green, x_n = 60); simulated with *k*MC with *ca.* 10^8 chains. Conditions: Top: entry 3 in Table S1;† Bottom: entry 3 in Table S2;† model parameters: Table S3.†

Below the white dashed line the dormant chains are depicted and above this line the dead chains. In agreement with the previous results and discussions, it follows that most chains are dormant as the majority of chains are below the white dashed line. A more detailed analysis shows that a significant part of the dormant and dead chains have the undesired I end-group, confirming the difficult R_0X consumption. Clearly, a high scatter in chain lengths is obtained with in particular a strong deviation in the contribution of the dormant and dead macrospecies which are, respectively, shorter and longer than the mean value (x_n = 51).

Microstructural control upon chain extension with styrene

As explained above, an efficient R_0X removal is obtained without altering the original SEC trace upon dialysis of the homopolymer. Consequently, by the addition of fresh styrene and AIBN to the purified polymer, potential chain extension can be investigated. Importantly, k_{tr} is then the only relevant transfer rate coefficient as exclusively styrene macrospecies are present. Hence, by regression analysis based on X_m, x_n, x_m, and $Đ$ data from chain extension experiments (points in Fig. 11; 70 °C) this RAFT exchange parameter can be estimated.

As shown in Fig. S15 of the ESI,† the most valuable data for this parameter tuning are the x_m and $Đ$ data, resulting in k_{tr} = (2.1 ± 0.4) × 10^2 L mol^{-1} s^{-1}. The corresponding C_{tr} reaches a value of 0.44 ± 0.07. Narrow confidence intervals are thus obtained for the macro-RAFT exchange kinetic parameters, which is reflected in the good agreement between the experimental and deterministic simulation results in Fig. 11. Notably, the obtained k_{tr} (eqn (3)) value is 45% lower than the estimated $k_{tr,0}$ (eqn (1)) value of (3.8 ± 0.1) × 10^2 L mol^{-1} s^{-1}. This lowering is kinetically significant as demonstrated in Fig. S15 in the ESI† in which different simulation results of several polymer characteristics are obtained in case k_{tr} is assumed to be equal to $k_{tr,0}$.

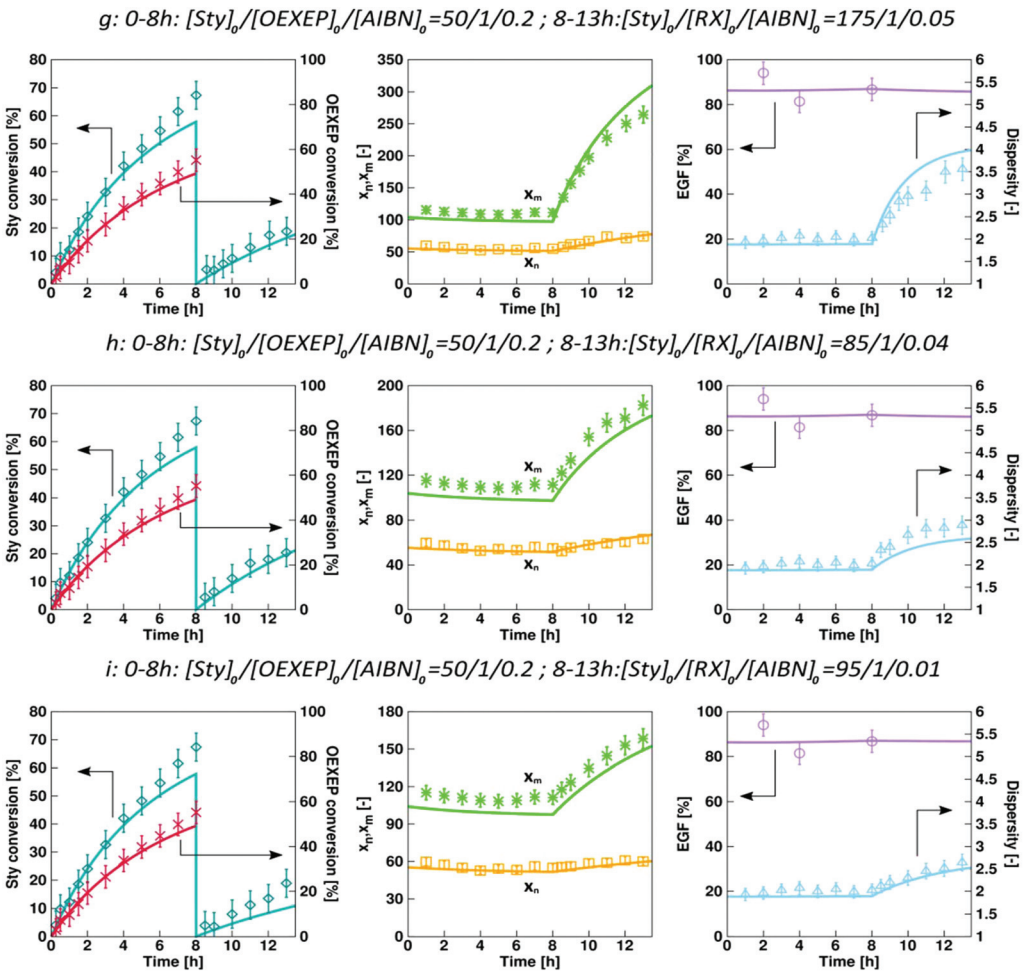

Fig. 11 Comparison of simulated and experimental data for MADIX homopolymerization of styrene (0–8 h; entry 3 in Table S1 in the ESI†) and subsequent chain extension of (dormant) polystyrene (after purification *via* dialysis) with fresh styrene (8–13 h; entries 1–3 in Table S2 in the ESI†); 70 °C; monomer conversion (X_m, dark blue), R_0X conversion (X_{R0X}, red), number-average chain length (x_n, orange), mass-average chain length (x_m, green), dispersity ($Đ$, purple), and end-group functionality (EGF, light blue) as a function of time; lines correspond to calculated values with rate coefficients given in Table S3 in ESI† and accounting for diffusional limitations (parameters in Table S4†); simulated output with the deterministic method.

Fig. 12 Exchange (2) in Fig. 6 at the elementary level. Interpretation of eqn (1) starting from the estimated value for $k_{tr,0}$ with the kinetic model.

Based on eqn (3) it further follows that $k_{add} = 2k_{tr} = 4.2 \times 10^2$ L mol^{-1} s^{-1} (70 °C). Keeping in mind that $k_{tr,0}$ is, on a fundamental level, related to the addition and fragmentation reactions in Fig. 12 also here further mechanistic insights can be obtained *a posteriori*, based on eqn (1). If it is assumed that $k_{add,0,a}$ (RAFT addition of R_i to R_0X) is equal to k_{add}, consistent with the common claim that the RAFT addition rate coefficient is mainly influenced by the nature of the Z group, it follows from eqn (1) that the fragmentation probability $\varphi_{0,b}$ for the intermediate R_0XR_I toward R_0 is equal to 0.9 (see also Table S3 in the ESI†). The latter is unexpected as this would imply a much higher stability for R_0 (bond dissociation energy[105] of $R_0 - H$ = 394 kJ mol^{-1}) compared to the secondary benzylic R_i radical (bond dissociation energy[106] of $R_i - H$ = 354–378 kJ mol^{-1}). It is more plausible thus to assume that $\varphi_{0,b}$ is lower than 0.9 resulting in a $k_{add,0,a}$ higher than k_{add}. Hence, both the Z and R groups are important in determining the RAFT addition reactivity and by extension the overall transfer coefficient. Nonetheless, the Z group remains paramount as it determines the order of magnitude of $k_{tr(,0)}$ as for instance demonstrated by the difference for xanthates and trithiocarbonates in combination with LAMs/MAMs.

Further inspection of Fig. 11 shows that the chain extension with fresh styrene results in an increase of x_n, x_m and $Đ$ while having a negligible effect on EGF. This weak dependence for EGF is due to the relatively small number of newly formed dead chains. The latter can be most easily derived from Fig. 10 (bottom) which shows the explicit growth of the chains as accessible *via* the *k*MC simulations (conditions: entry 3 in Table S2 in the ESI†) with the freshly incorporated styrene units in green colour and again making a distinction between the different end-groups. As can be seen, the fresh styrene is mainly incorporated in the macroradicals formed by the activation of the dormant species originating from the first synthesis step and much more "block"-copolymer chains are present than "green" homopolymer chains. Again a single (net) transfer, as countable *via* the *k*MC simulations,[107] takes place similar to the reaction scheme shown in Fig. 6 with R_0X replaced by the dormant macrospecies (RX), taking into account the fact that the additional styrene conversion remains sufficiently low (Fig. 11).

The accuracy of the determination of $k_{tr,0}$ and k_{tr} is further confirmed in the SEC traces in Fig. 13 which show good agreement between the experimental and simulated mass CLD after 8 h of homopolymerization (green; X_m = 65%; entry 3 in the ESI Table S1†) and subsequent 5 h of chain extension with fresh styrene (blue; X_m = 20%; entry 1 in the ESI Table S2†). A high molar mass shoulder is present after the chain extension, consistent with the simulations results in Fig. 10 (bottom).

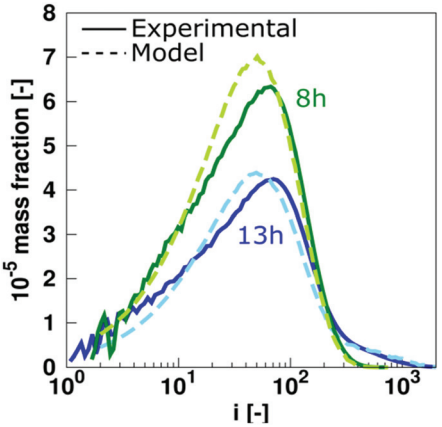

Fig. 13 Comparison of the experimental (full lines) and simulated (dashed lines) mass CLD after 8 h of homopolymerization (green; X_m = 65%; entry 3 in the ESI Table S1†) and subsequent 5 h of chain extension with fresh styrene (blue; X_m = 20%; entry 1 Table S2 in the ESI†).

Consequently, although no typical RDRP control over the chain growth is possible, reactivation of the dormant species can still be achieved under the right circumstances, *i.e.* upon R_0X removal.

Microstructural control upon chain extension with *n*BuA

To further illustrate the potential of the visualization tool, our focus is on a second monomer in view of the synthesis of actual block copolymer chains. Not any monomer can be selected, as the intermediate formed by exchange between the dormant species consisting of the first monomer (here styrene) and the macroradicals consisting of the second monomer must effectively fragment toward macroradicals of the first monomer type. An efficient reinitiation involving these radicals with the second monomer is needed as well to allow for chain extension and, hence, block copolymer formation.[108]

Based on the experimental work of Smulders *et al.*[30], *n*BuA is an interesting monomer. For example, Fig. 14 (top) shows the model description of the experimental dispersity data[30] for the chain extension in toluene of dormant polystyrene synthesized with OEXEP. The corresponding simulated monomer sequences are provided in Fig. 14 (bottom). Based on the literature data and for simplicity, backbiting and thus short chain branching are neglected.[109]

For the simulations in Fig. 14, at first sight, four macro-RAFT exchange reactions are needed due to the possible presence of two macroradical and dormant species types, with either a styrene or an *n*BuA terminal unit. Mathematically, this implies an extension of eqn (3) through the introduction of $k_{tr,XY}$ with X referring to the radical terminal unit and Y to the dormant terminal unit ($k_{tr,nB,nB}$; $k_{tr,nB,S}$; $k_{tr,S,S}$; $k_{tr,S,nB}$; S: styrene; *n*B: *n*BuA). However, as shown in Fig. S16 in the ESI and as explained in detail in section S23 of the ESI,† for the low *n*BuA conversions as covered in the present work (≤45%), only the transfer coefficient for a macroradical with a *n*BuA

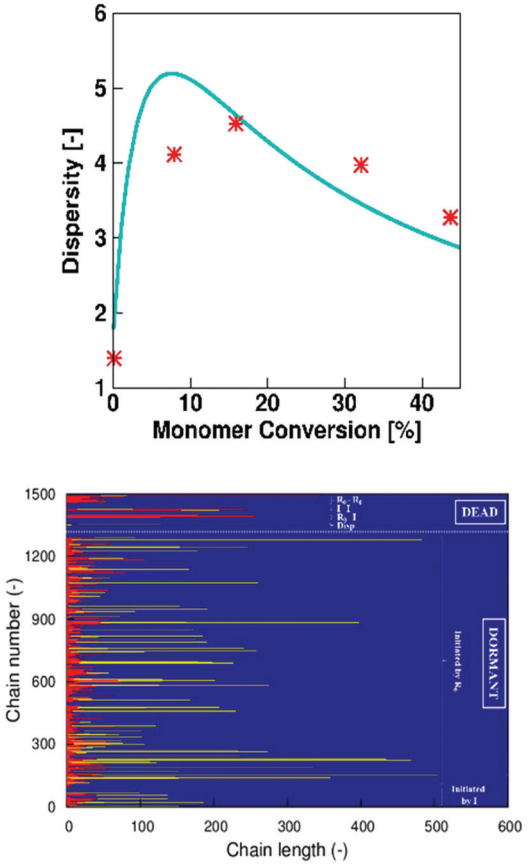

Fig. 14 Top: Comparison of simulated (blue) and experimental (red) dispersity data[30] for MADIX chain extension of dormant polystyrene with *n*-butyl acrylate; reaction conditions: $[\text{toluene}]_0$ = 6 mol L^{-1}, $[n\text{-BuA}]_0$ = 2.0 mol L^{-1}, $[n\text{-BuA}]_0/[R_{i,sty}X]_0/[\text{AIBN}]_0$ = 198/1/1; T = 60 °C; bottom: visualization of monomer sequences using kinetic Monte Carlo modelling after 20% monomer conversion of chain extension: red: styrene unit; yellow: *n*-butyl acrylate; parameters: Table S6 of the ESI.†

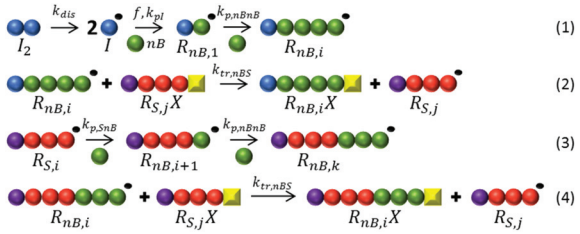

Fig. 15 Kinetically relevant MADIX reactions (termination by recombination/disproportionation not shown for simplicity) for the chain extension of dormant polystyrene (after dialysis to remove OEXEP) with *n*BuA up to intermediate conversions; $R_{nB/S}$: macroradical with *n*-butyl acrylate (nB; green spheres) or styrene (S; red spheres) as the terminal unit. Similar notation for dormant species.

terminal unit and a dormant species with a styrene terminal unit ($k_{tr,nBS}$) can be seen as kinetically significant. Styryl macroradicals which have been formed by activation of the original dormant polystyrene chains have already reacted with *n*BuA before RAFT exchange can occur, due to the typical low k_{tr} values for xanthates in combination with MAMs. Hence, only *n*BuA terminal radicals are present, which reduces the number of exchange reactions already safely from 4 to 2 (the remaining rate coefficients: $k_{tr,nBS}$ and $k_{tr,nBnB}$). Furthermore, due to the low concentration of dormant poly(styrene-*block*-*n*BuA) compared to the initial dormant polystyrene at low *n*BuA conversions, transfer of *n*BuA macroradicals with the dormant block copolymer species ($k_{tr,nBnB}$) is less relevant and can be neglected (Fig. S17 in the ESI†). Supportive for this claim is also the expectation that $k_{tr,nB,nB}$ is lower than $k_{tr,nB,S}$, taking into account the fact that the bond dissociation energy[110] of the benzylic C–H bond of ethyl benzene (354–378 kJ mol^{-1}) is lower than that of the C–H bond at the alpha position of ethyl propionate (400 kJ mol^{-1}).[110] This implies that $k_{tr,nB,S}$ can be seen as the only kinetically relevant RAFT transfer coefficient, at least to a first approximation. The resulting simplified reaction scheme is shown in Fig. 15, considering all kinetically relevant MADIX reactions for the chain extension of dormant polystyrene with *n*BuA up to intermediate conversion.

Based on the data in Fig. 14 (top), a preliminary value of 4.6×10^4 L mol^{-1} s^{-1} results for $k_{tr,nBS}$, which corresponds to a $C_{tr,nB,S}$ equal to 1.35, in agreement with the kinetic study by Smulders *et al.*[30] Such a C_{tr} value can still be seen as relatively low but suffices to enable a successful MADIX chain extension, as confirmed by the *k*MC simulation results in Fig. 14 (bottom).

Conclusions

A detailed understanding of MADIX under bulk/solution conditions is obtained by successfully combining experimental and modelling analysis tools, focusing on conversion, chain length and EGF data. The latter data can be obtained by a combination of dialysis and elemental analyses, an insight relevant for all RAFT polymerizations and, hence, not restricted to exchange processes based on xanthates.

To accurately estimate $C_{tr,0}$ for the OEXEP/styrene MADIX system, applying multi-response regression analysis to homopolymerization data is recommended. On the other hand, C_{tr} can be reliably estimate from specifically x_m data upon polymer isolation, using dialysis and applying chain extension. For OEXEP and styrene, $C_{tr,0}$ and C_{tr} of 0.80 ± 0.02 and 0.44 ± 0.07, respectively, result, highlighting the influence of both the R and Z groups of the agent on the RAFT addition and fragmentation coefficients. For chain extension with *n*BuA, a C_{tr} of 1.35 is put forward in the present work, reflecting the reactivity for RAFT exchange of macroradicals with an *n*BuA terminal unit and dormant macrospecies with a styrene terminal unit.

The use of advanced kinetic Monte Carlo simulations enables visualization of the chain growth and end-groups of individual macrospecies, both during homopolymerization and chain extension. For the selected MAM systems and monomer conversions, the dormant macrospecies are always

formed *via* a single exchange, which implies a transfer behaviour as in a conventional free radical polymerization, although with a slight delay due to the reversible nature of the first addition/fragmentation step. Hence, bulk MADIX with MAMs behaves mechanistically different from classical bulk RAFT polymerizations with consecutive well-defined activation–growth–deactivation cycles.

Conflicts of interest

There are no conflicts of interest to declare.

Acknowledgements

D. J. G. D., P. H. M. V. S., L. D. K., M.-F. R., and D. R. D. acknowledge financial support from the Long Term Structural Methusalem Funding by the Flemish Government, the Interuniversity Attraction Poles Programme, and the Fund for Scientific Research Flanders (FWO; G.0065.13N). D. R. D. and P. H. M. V. S. acknowledge the FWO through a postdoctoral fellowship.

References

1 J. Chiefari, Y. K. B. Chong, F. Ercole, J. Krstina, J. Jeffery, T. P. T. Le, R. T. A. Mayadunne, G. F. Meijs, C. L. Moad, G. Moad, E. Rizzardo, S. H. Thang and C. South, *Macromolecules*, 1998, **31**, 5559–5562.
2 G. Gody, T. Maschmeyer, P. B. Zetterlund and S. Perrier, *Macromolecules*, 2014, **47**, 3451–3460.
3 G. Gody, T. Maschmeyer, P. B. Zetterlund and S. Perrier, *Macromolecules*, 2014, **47**, 639–649.
4 X. Zhang, S. Boissé, W. Zhang, P. Beaunier, F. D'Agosto, J. Rieger and B. Charleux, *Macromolecules*, 2011, **44**, 4149–4158.
5 C. Barner-kowollik, *Handbook of RAFT Polymerization*, Wiley-VCH, Weinheim, 2008.
6 P. Lebreton, B. Ameduri, B. Boutevin and J. M. Corpart, *Macromol. Chem. Phys.*, 2002, **203**, 522–537.
7 M. M. Adamy, A. M. van Herk, M. Destarac and M. J. Monteiro, *Macromolecules*, 2003, **36**, 2293–2301.
8 P. Derboven, P. Van Steenberge, M.-F. Reyniers, C. Barner-Kowollik, D. R. D'hooge and G. B. Marin, *Polym. Chem.*, 2016, **7**, 3334–3349.
9 Y. Kwak, A. Goto, Y. Tsujii, Y. Murata, K. Komatsu and T. Fukuda, *Macromolecules*, 2002, **35**, 3026–3029.
10 Y. Kwak, A. Goto and T. Fukuda, *Macromolecules*, 2004, **37**, 1219–1225.
11 N. De Rybel, P. H. M. Van Steenberge, M.-F. Reyniers, C. Barner-Kowollik, D. R. D'hooge and G. B. Marin, *Macromol. Theory Simul.*, 2017, **26**, 1600048.
12 D. Konkolewicz, B. S. Hawkett, A. Gray-Weale and S. Perrier, *Macromolecules*, 2008, **41**, 6400–6412.
13 C. Barner-Kowollik and S. Perrier, *J. Polym. Sci., Part A: Polym. Chem.*, 2008, **46**, 5715–5723.
14 C. Barner-Kowollik, J. F. Quinn, D. R. Morsley and T. P. Davis, *J. Polym. Sci., Part A: Polym. Chem.*, 2001, **39**, 1353–1365.
15 J. Chiefari, R. T. A. Mayadunne, C. L. Moad, G. Moad, E. Rizzardo, A. Postma, M. A. Skidmore and S. H. Thang, *Macromolecules*, 2003, **36**, 2273–2283.
16 B. Y. K. Chong, J. Krstina, T. P. T. Le, G. Moad, A. Postma, E. Rizzardo and S. H. Thang, *Macromolecules*, 2003, **36**, 2256–2272.
17 M. Destarac, *Polym. Rev.*, 2011, **51**, 163–187.
18 *Controlled Radical Polymerization: Mechanisms*, ed. K. Matyjaszewski, B. S. Sumerlin, N. V. Tsarevsky and J. Chiefari, American Chemical Society, 2015.
19 G. Moad, E. Rizzardo and S. H. Thang, *Aust. J. Chem.*, 2012, **65**, 985–1076.
20 P. Derboven, P. H. M. Van Steenberge, M. Reyniers, C. Barner-kowollik, D. R. D'hooge and G. B. Marin, *Macromol. Theory Simul.*, 2016, **25**, 104–115.
21 M. R. Hill, R. N. Carmean and B. S. Sumerlin, *Macromolecules*, 2015, **48**, 5459–5469.
22 S. Perrier and P. Takolpuckdee, *J. Polym. Sci., Part A: Polym. Chem.*, 2005, **43**, 5347–5393.
23 L. Seiler, J. Loiseau, F. Leising, P. Boustingorry, S. Harrisson and M. Destarac, *Polym. Chem.*, 2017, **8**, 3825–3832.
24 E. Rizzardo and D. H. Solomon, *Aust. J. Chem.*, 2012, **65**, 945–969.
25 A. Ilchev, R. Pfukwa, L. Hlalele, M. Smit and B. Klumperman, *Polym. Chem.*, 2015, **6**, 7945–7948.
26 G. Pound, J. B. McLeary, J. M. McKenzie, R. F. M. Lange and B. Klumperman, *Macromolecules*, 2006, **39**, 7796–7797.
27 G. Pound, F. Aguesse, J. B. McLeary, R. F. M. Lange and B. Klumperman, *Macromolecules*, 2007, **40**, 8861–8871.
28 I. Van Nieuwenhove, S. Maji, M. Dash, S. Van Vlierberghe, R. Hoogenboom and P. Dubruel, *Polym. Chem.*, 2017, **8**, 2433–2437.
29 M. H. Stenzel, L. Cummins, G. E. Roberts, T. P. Davis, P. Vana and C. Barner-Kowollik, *Macromol. Chem. Phys.*, 2003, **204**, 1160–1168.
30 W. Smulders and M. J. Monteiro, *Macromolecules*, 2004, **37**, 4474–4483.
31 P. Corpart, D. Charmot, T. Biadatti, S. Z. Zard and D. Michelet, *WO* 1998058974, 1998.
32 W. Smulders, R. G. Gilbert and M. J. Monteiro, *Macromolecules*, 2003, **36**, 4309–4318.
33 M. J. Monteiro and J. De Barbeyrac, *Macromolecules*, 2001, **34**, 4416–4423.
34 M. P. F. Pepels, C. I. Holdsworth, S. Pascual and M. J. Monteiro, *Macromolecules*, 2010, **43**, 7565–7576.
35 G. Moad, J. Chiefari, Y. K. Chong, J. Krstina, R. T. A. Mayadunne, A. Postma, E. Rizzardo and S. H. Thang, *Polym. Int.*, 2000, **49**, 993–1001.
36 M. Destarac, W. Bzducha, D. Taton, I. Gauthier-Gillaizeau and S. Z. Zard, *Macromol. Rapid Commun.*, 2002, **23**, 1049–1054.

37 M. Destarac, C. Brochon, J. M. Catala, A. Wilczewska and S. Z. Zard, *Macromol. Chem. Phys.*, 2002, **203**, 2281–2289.
38 A. H. E. Muller, R. G. Zhuang, D. Y. Yan and G. Litvinenko, *Macromolecules*, 1995, **28**, 4326–4333.
39 F. R. Mayo, *J. Am. Chem. Soc.*, 1943, **65**, 2324–2329.
40 P. A. Clay and R. G. Gilbert, *Macromolecules*, 1995, **28**, 552–569.
41 A. Goto, T. Terauchi, T. Fukuda and T. Miyamoto, *Macromol. Rapid Commun.*, 1997, **18**, 673–681.
42 T. Fukuda and A. Goto, *Macromol. Rapid Commun.*, 1997, **18**, 683–688.
43 A. Goto, K. Sato, Y. Tsujii, T. Fukuda, G. Moad, E. Rizzardo and S. H. Thang, *Macromolecules*, 2001, **34**, 402–408.
44 S. W. Prescott, M. J. Ballard, E. Rizzardo and R. G. Gilbert, *Aust. J. Chem.*, 2002, **55**, 415.
45 M. F. Cunningham, *Prog. Polym. Sci.*, 2008, **33**, 365–398.
46 P. B. Zetterlund, *Polym. Chem.*, 2011, **2**, 534–549.
47 P. B. Zetterlund, S. C. Thickett, S. Perrier, E. Bourgeat-Lami and M. Lansalot, *Chem. Rev.*, 2015, **115**, 9745–9800.
48 P. B. Zetterlund, Y. Kagawa and M. Okubo, *Chem. Rev.*, 2008, **108**, 3747–3794.
49 J. M. Asua, *Prog. Polym. Sci.*, 2014, **39**, 1797–1826.
50 E. Mastan, X. Li and S. Zhu, *Prog. Polym. Sci.*, 2015, **45**, 71–101.
51 D. R. D'hooge, P. H. M. Van Steenberge, M.-F. Reyniers and G. B. Marin, *Prog. Polym. Sci.*, 2016, **58**, 59–89.
52 M. J. Monteiro and M. F. Cunningham, *Macromolecules*, 2012, **45**, 4939–4957.
53 M. J. Monteiro, *J. Polym. Sci., Part A: Polym. Chem.*, 2005, **43**, 5643–5651.
54 Y. Luo, R. Wang, L. Yang, B. Yu, B. Li and S. Zhu, *Macromolecules*, 2006, **39**, 1328–1337.
55 I. S. Altarawneh, V. G. Gomes and M. S. Srour, *Macromol. React. Eng.*, 2008, **2**, 58–79.
56 S. M. Jung and V. G. Gomes, *Macromol. React. Eng.*, 2011, **5**, 303–315.
57 D. R. D'hooge, P. H. M. Van Steenberge, P. Derboven, M.-F. Reyniers and G. B. Marin, *Polym. Chem.*, 2015, **6**, 7081–7096.
58 P. H. M. Van Steenberge, D. R. D'hooge, M. F. Reyniers, G. B. Marin and M. F. Cunningham, *Macromolecules*, 2014, **47**, 7732–7741.
59 Y. N. Zhou, C. M. Guan and Z.-H. Luo, *Eur. Polym. J.*, 2010, **46**, 2164–2173.
60 Z.-H. Luo, X.-L. Zhan and Y.-R. Yang, *J. Shanghai Univ.*, 2006, **10**, 274–276.
61 W. W. Smulders, *Macromolecular Architecture in Aqueous Dispersions: "living" free radical polymerization in emulsion*, Technische Universiteit Eindhoven, 2002.
62 J. Vandenbergh and T. Junkers, *Macromolecules*, 2014, **47**, 5051–5059.
63 J. C. Bevington, J. R. Ebdon and T. N. Huckerby, *Eur. Polym. J.*, 1985, **21**, 685–694.
64 C. Lefay, J. Belleney, B. Charleux, O. Guerret and S. Magnet, *Macromol. Rapid Commun.*, 2004, **25**, 1215–1220.
65 J. C. Bevington and T. N. Huckerby, *Eur. Polym. J.*, 2006, **42**, 1433–1436.
66 A. Postma, T. P. Davis, A. R. Donovan, G. Li, G. Moad, R. Mulder and M. S. O'Shea, *Polymer*, 2006, **47**, 1899–1911.
67 J.-F. Lutz and K. Matyjaszewski, *J. Polym. Sci., Part A: Polym. Chem.*, 2005, **43**, 897–910.
68 K. Matyjaszewski, S. M. Jo, H. Paik and D. A. Shipp, *Macromolecules*, 1999, **32**, 6431–6438.
69 H. Willcock and R. K. O'Reilly, *Polym. Chem.*, 2010, **1**, 149.
70 M. Rodlert, E. V. A. Harth, I. A. N. Rees and C. J. Hawker, *J. Polym. Sci., Part A: Polym. Chem.*, 2000, **38**, 4749–4763.
71 M. Dourges, B. Charleux, J. Vairon and J. Tabet, *Macromolecules*, 1999, **32**, 2495–2502.
72 M. Bednarek, T. Biedron and P. Kubisa, *Macromol. Chem. Phys.*, 2000, **201**, 58–66.
73 S. O. Hammouch and J. Catala, *Macromol. Rapid Commun.*, 1996, **17**, 149–154.
74 M. J. Monteiro, M. M. Adamy, B. J. Leeuwen, A. M. van Herk and M. Destarac, *Polym. Prepr. (Am. Chem. Soc., Div. Polym. Chem.)*, 2005, **46**, 353–354.
75 M. J. Monteiro, M. Sjöberg, J. Van Der Vlist and C. M. Göttgens, *J. Polym. Sci., Part A: Polym. Chem.*, 2000, **38**, 4206–4217.
76 J. D. Woloszyn and K. B. Mcauley, *Macromol. React. Eng.*, 2011, **5**, 453–466.
77 P. Derboven, P. H. M. Van Steenberge, M. Reyniers, C. Barner-kowollik, R. D. Dagmar and G. B. Marin, *Macromol. Theory Simul.*, 2016, **25**, 104–115.
78 E. Mastan and S. Zhu, *Eur. Polym. J.*, 2015, **68**, 139–160.
79 D. R. D'hooge, M.-F. Reyniers and G. B. Marin, *Macromol. React. Eng.*, 2009, **3**, 185–209.
80 D. R. D'hooge, M. F. Reyniers and G. B. Marin, *Macromol. React. Eng.*, 2013, **7**, 362–379.
81 W. Wang, Y. Zhou, L. Shi and Z.-H. Luo, *Ind. Eng. Chem. Res.*, 2014, **53**, 11873–11883.
82 Y.-N. Zhou and Z.-H. Luo, *Macromol. React. Eng.*, 2016, **10**, 516–534.
83 D. T. Gillesple, *J. Phys. Chem.*, 1977, **81**, 2340–2361.
84 P. H. M. Van Steenberge, D. R. D'hooge, M.-F. Reyniers and G. B. Marin, *Chem. Eng. Sci.*, 2014, **110**, 185–199.
85 P. H. M. Van Steenberge, D. R. D'hooge, Y. Wang, M. Zhong, M.-F. Reyniers, D. Konkolewicz, K. Matyjaszewski and G. B. Marin, *Macromolecules*, 2012, **45**, 8519–8531.
86 R. H. Byrd, P. T. Boggs, J. E. Rogers and R. B. Schnabel, *ODRPACK Software for Orthogonal Distance Regression*, 1992.
87 I. Chavez-Sumarriva, P. H. M. Van Steenberge and D. R. D'hooge, *Ind. Eng. Chem. Res.*, 2016, **55**, 9387–9396.
88 C. Toloza Porras, D. R. D'hooge, P. H. M. Van Steenberge, M. F. Reyniers and G. B. Marin, *Ind. Eng. Chem. Res.*, 2014, **53**, 9674–9685.
89 A. Theis, T. P. Davis, M. H. Stenzel and C. Barner-Kowollik, *Polymer*, 2006, **47**, 999–1010.
90 P. Vana, T. P. Davis and C. Barner-Kowollik, *Macromol. Rapid Commun.*, 2002, **23**, 952–956.

91 G. Johnston-Hall, M. H. Stenzel, T. P. Davis, C. Barner-Kowollik and M. J. Monteiro, *Macromolecules*, 2007, **40**, 2730–2736.
92 P. Derboven, D. R. D'hooge, M.-F. Reyniers, G. B. Marin and C. Barner-Kowollik, *Macromolecules*, 2015, **48**, 492–501.
93 T. Junkers, A. Theis, M. Buback, T. P. Davis, M. H. Stenzel, P. Vana and C. Barner-Kowollik, *Macromolecules*, 2005, **38**, 9497–9508.
94 G. Johnston-Hall, A. Theis, M. J. Monteiro, T. P. Davis, M. H. Stenzel and C. Barner-Kowollik, *Macromol. Chem. Phys.*, 2005, **206**, 2047–2053.
95 A. Theis, T. P. Davis, M. H. Stenzel and C. Barner-Kowollik, *Macromolecules*, 2005, **38**, 10323–10327.
96 A. Theis, A. Feldermann, N. Charton, T. P. Davis, M. H. Stenzel and C. Barner-Kowollik, *Polymer*, 2005, **46**, 6797–6809.
97 A. Theis, A. Feldermann, N. Charton, M. H. Stenzel, T. P. Davis and C. Barner-kowollik, *Macromolecules*, 2005, **38**, 2595–2605.
98 A. Feldermann, M. H. Stenzel, T. P. Davis, P. Vana and C. Barner-Kowollik, *Macromolecules*, 2004, **37**, 2404–2410.
99 S. K. Fierens, P. H. M. Van Steenberge, M.-F. Reyniers, D. R. D'hooge and G. B. Marin, *AIChE J.*, 2017, **63**, 4971–4986.
100 A. M. Rabea and S. Zhu, *Polymer*, 2015, **7**, 819–835.
101 G. Johnston-Hall and M. J. Monteiro, *J. Polym. Sci., Part A: Polym. Chem.*, 2008, **46**, 3155–3176.
102 G. Johnston-Hall and M. J. Monteiro, *Macromolecules*, 2017, **40**, 7171–7179.
103 R. V. Hogg, A. Craig and J. W. McKean, *Introduction to Mathematical Statistics*, 6th edn, 2005.
104 G. Odian, *Principles of Polymerization*, John Wiley & Sons, New Jersey, 2004.
105 A. M. El-Nahas, M. V. Navarro, J. M. Simmie, J. W. Bozzelli, H. J. Curran, S. Dooley and W. Metcalfe, *J. Phys. Chem. A*, 2007, **111**, 3727–3739.
106 A. O'Mally and B. K. Hodnett, *Stud. Surf. Sci. Catal.*, 1997, **110**, 1137–1144.
107 S. K. Fierens, S. Telitel, P. H. M. Van Steenberge, M.-F. Reyniers, G. B. Marin, J.-F. Lutz and D. R. D'hooge, *Macromolecules*, 2016, **49**, 9336–9344.
108 D. J. Keddie, *Chem. Soc. Rev.*, 2014, **43**, 496–505.
109 D. Konkolewicz, S. Sosnowski, R. D. Dagmar, R. Szymanski, G. B. Marin and K. Matyjaszewski, *Macromolecules*, 2011, **44**, 8361–8373.
110 Y.-R. Luo, *Handbook of Bond Dissociation Energies in Organic Compounds*, CRC Press, 2003.